Isotope shifts and hyperfine structure in the 369.4-nm $6s$-$6p_{1/2}$ resonance line of singly ionized ytterbium

Ann-Marie Mårtensson-Pendrill
Department of Physics, Chalmers University of Technology, S-412 96 Göteborg, Sweden

David S. Gough and Peter Hannaford*
Division of Materials Science and Technology, Commonwealth Scientific and Industrial Research Organization, Rosebank MDC, Clayton, Victoria 3169, Australia

(Received 3 December 1993)

Isotope shifts and hyperfine structure in the 369.4-nm $6s$-$6p_{1/2}$ resonance line of the single-valence-electron system Yb^+ have been determined with an accuracy of about 1 MHz by Doppler-free saturated absorption spectroscopy in a sputtered vapor. *Ab initio* many-body perturbation theory calculations in the coupled-cluster approach were then used to evaluate the electronic field shift factor, $F=-14.9(2)$ GHz fm^{-2}, and to estimate the specific mass shift (SMS) factor, $K^{\mathrm{SMS}}=(1\pm1)K^{\mathrm{NMS}}$, where NMS is the normal mass shift. The uncertainty in the calculated F factor is based on the level of agreement between the hyperfine structure constants calculated for $6s$ and $6p_{1/2}$ states using the same wave functions as for the F-factor calculation and the experimentally determined hyperfine-structure constants. The calculated F and K^{SMS} factors have been used to extract values for the difference in mean-square charge radius, $\delta\langle r^2\rangle^{A_1,A_2}$, between isotope pairs A_1, A_2, and the related nuclear charge distribution parameter λ^{A_1,A_2}, which are just within the uncertainties of the tabulated values of Aufmuth *et al.* [At. Data Nucl. Data Tables **37**, 455 (1987)] based on semiempirical estimates of F and assumed values of K^{SMS}.

PACS number(s): 31.30.Gs, 35.10.Fk, 21.10.Ft

I. INTRODUCTION

Isotope shifts in the *ns-np* resonance lines of single-valence-electron systems such as Ca^+, Ba^+, and Yb^+ are of special interest because such systems are now amenable to *ab initio* many-body perturbation theory (MBPT) that allows calculations of the electronic field shift (FS) factor $F_{ns\text{-}np}$ and the specific mass shift (SMS) factor K^{SMS} [1–3]. Knowledge of the electronic FS and SMS factors then permits a full analysis of the experimental isotope shifts for the *ns-np* transition, and hence values of the nuclear charge distribution parameters λ^{A_1,A_2} and $\delta\langle r^2\rangle^{A_1,A_2}$ for isotope pairs A_1, A_2 to be extracted from the experimental isotope shifts. This information in turn allows electronic FS and SMS factors to be deduced from the isotope shift data for any other transition in the same element, and also λ^{A_1,A_2} and $\delta\langle r^2\rangle^{A_1,A_2}$ values to be deduced for any additional isotope pairs (e.g., involving rare or radioactive isotopes) for which isotope shift data are available.

Previous analyses of optical isotope shifts in ytterbium have been based mainly on transitions in neutral ytterbium, for which semiempirical estimates of the electronic FS factor and assumed values of the SMS have been used [4,5]. The different investigations have yielded sets of λ^{A_1,A_2} or $\delta\langle r^2\rangle^{A_1,A_2}$ values that differ by about 30%. It would seem that the isotope shift analysis for ytterbium could be improved substantially by utilizing experimental isotope shift data for one of the Yb^+ $6s$-$6p$ transitions together with MBPT calculations to evaluate the electronic FS and SMS factors. Although moderately accurate [$\pm$(10–30) MHz] isotope shift data exist for the Yb^+ 328.9-nm $6s$-$6p_{3/2}$ transition [6], we find that the perturbation expansion for the Yb^+ $6p_{3/2}$ state converges slowly on account of the proximity of a $4f^{13}5d6s\ J=\frac{3}{2}$ state [see Fig. 1(a)] just below the $6p_{3/2}$ state, and in particular our attempted calculation of the FS factor for the $6p_{3/2}$ state shows no sign of convergence. The only reported isotope shift data for the 369.4-nm $6s$-$6p_{1/2}$ transition are the very early Doppler-limited results of Krebs and Nelkowski [7], Golovin and Striganov [8], and Chaiko [9].

In this paper we report Doppler-free saturated absorption measurements of isotope shifts and hyperfine structure in the Yb^+ 369.4-nm $6s$-$6p_{1/2}$ resonance line. The vapor of Yb^+ ions was produced by cathodic sputtering in a low-pressure rare-gas discharge, and the narrow-band 369.4-nm radiation was generated by intracavity frequency doubling of an actively stabilized titanium:sapphire ring laser. The experimental details of the saturated absorption measurements are described in Sec. II, and the isotope shift and hyperfine-structure results presented in Sec. III. The isotope shift and hyperfine-structure data, which represent one to two orders of magnitude improvement in accuracy over earlier results, complement the accurate hyperfine-structure results for the $6s$ ground state obtained recently by microwave-optical double-resonance spectroscopy [10–12]. Information on isotope shifts and hyperfine structure in the 349.4-nm $6s$-$6p_{1/2}$ transition should be of

*Electronic address: hannafor@rivett.csiro.mst.au

interest to a number of groups who are currently using this transition for laser-cooling Yb^+ ions confined in electromagnetic traps, with the aim of developing new atomic clocks in the microwave and optical regimes [6,10–14].

The relativistic generalization of the coupled-cluster approach [15], including single and double excitations, has been applied to the 6*s* and 6*p* states of Yb^+, and the resulting wave functions used to evaluate the FS factors, $F_{6s\text{-}6p}$, for the 6*s*-6*p* transitions and the hyperfine interaction constants for the 6*s* and 6*p* states in $^{171}Yb^+$ and $^{173}Yb^+$. In practice, the 14 easily perturbed 4*f* core electrons make these states very sensitive to correlation effects, and it is found that the inclusion of double excitations may not be sufficient, particularly for the $6p_{3/2}$ state. For heavy elements such as Yb, the mass shift is much smaller than the FS, but is still not completely negligible. In order to allow a more detailed interpretation of the isotope shift data, a lowest-order calculation of the SMS has also been performed, essentially analogous to that by Hartley and Mårtensson-Pendrill [3] for Cs and Tl. However, the SMS is, in general, very sensitive to correlation effects, and uncertainties in the SMS are presently a limiting factor in the analysis of the Yb^+ isotope shift data presented here. The details of the calculations of the electronic FS and SMS factors are presented in Sec. IV.

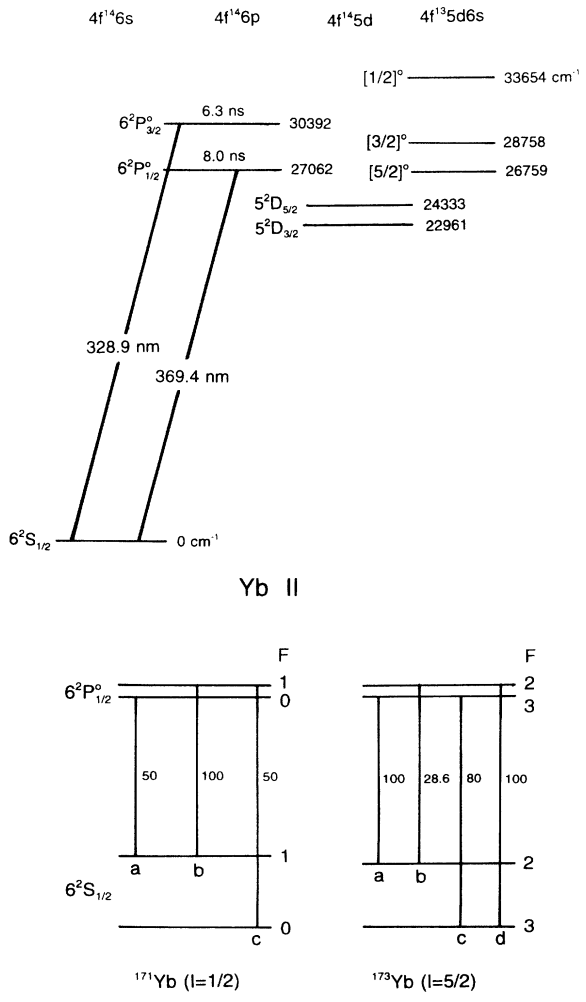

FIG. 1. (a) Partial energy-level diagram for Yb II, showing the two main resonance lines, at 369.4 and 328.9 nm. Lifetimes are taken from Ref. [23]. (b) Hyperfine transitions for the 369.4-nm $6s\text{-}6p_{1/2}$ resonance line in $^{171}Yb^+$ and $^{173}Yb^+$.

The calculated electronic FS and SMS factors have been used to extract values of the nuclear charge distribution parameters λ^{A_1,A_2} and $\delta\langle r^2\rangle^{A_1,A_2}$ for isotope pairs involving the stable isotopes $^{170-174,176}Yb$ from the experimental 369.4-nm $6s\text{-}6p_{1/2}$ isotope shifts, and also for isotope pairs involving neutron-deficient radioactive isotopes down to the $N=82$ shell closure at ^{152}Yb, using the Yb I 555.6-nm isotope shift data of Clark *et al.* [4] Buchinger *et al.* [16], Sprouse *et al.* [17], and Billowes [18]. These results are presented in Sec. V.

II. EXPERIMENT

A. Experimental arrangement

The saturated absorption measurements were carried out using a sputtering discharge cell similar to that described in detail elsewhere [19]. It consists of a sealed Pyrex housing fitted with sidearms and windows and a demountable glass conical base with two tungsten pins onto which the cathode and anode are spot welded. The cathode comprises a small piece of natural ytterbium metal spot welded onto a zirconium plate of cross-sectional area about 0.3 cm^2. The discharge was operated in argon at pressures in the range 0.2–0.5 Torr and currents of 2–10 mA. An argon discharge was found to yield the highest densities of Yb^+ ions, which are generated by Penning collisions between the sputtered neutral ytterbium atoms and argon metastable atoms formed in the discharge.

The experimental arrangement for the saturated absorption measurements is similar to that described previously [20]. Two counter-propagating laser beams from a narrow-band tunable laser are directed into opposite ends of the sputtering cell. The pump beam is modulated by an acousto-optic modulator (AOM), and the transmission of the probe beam is detected by a photodiode coupled to a lock-in amplifier that is referenced to the modulation frequency of the AOM. The use of a high frequency of modulation (200 kHz) in the pump beam together with a low argon pressure (0.2 Torr) in the sputtering discharge resulted in almost total suppression of broad background pedestals caused by velocity-changing collisions between the Yb^+ ions and the argon atoms.

Tunable, single-frequency radiation at 369.4 nm was provided by second-harmonic generation in a $LiIO_3$ crystal mounted in an actively stabilized titanium:sapphire ring laser (Coherent 899-21). The UV output of the titanium:sapphire laser was typically 10 mW when pumped with 15-W multiline output from an argon-ion laser. The intensity of the pump laser beam in the saturated absorption measurements was about 0.2 $mW\,mm^{-2}$, and that of the probe beam about 0.02 $mW\,mm^{-2}$.

The frequency scale of the saturated absorption spectra was calibrated by simultaneously recording fringes from a

thermally stabilized confocal etalon at the fundamental laser wavelength 739 nm. The length of the etalon was determined to be 71.063(3) cm, which corresponds to a free spectral range of 105.439(5) MHz. The accurately known hyperfine splittings [10–12] in the 6*s* ground state of $^{171}Yb^+$ and $^{173}Yb^+$ served as a convenient internal calibration and yielded a value of 105.433(9) MHz. The latter result has been used in all frequency measurements reported here except the determination of the hyperfine structure of the 6*s* ground state for which the independently determined value of 105.439(5) MHz was used.

B. Saturated absorption spectrum of the Yb^+ 369.4-nm $6s$-$6p_{1/2}$ transition

A partial energy-level diagram for Yb^+, showing the main resonance lines at 369.4 and 328.9 nm, and the ^{171}Yb and ^{173}Yb hyperfine structure for the 369.4-nm line, is shown in Fig. 1.

The initial saturated absorption spectra were recorded with the laser pump beam chopped at a frequency of 100 kHz and the sputtering discharge operated at an argon pressure of 0.5 Torr [Fig. 2(a)]. The various isotopic components in these spectra were found to be very broad [$\approx$0.6 GHz full width at half maximum (FWHM) for the odd-isotope components] and the relative intensities appeared to bear little or no relationship to the intensities expected on the basis of the relative strengths of the ^{171}Yb and ^{173}Yb hyperfine components [Fig. 1(b)] and the known abundances of the Yb isotopes [0.135% ^{168}Yb, 3.03% ^{170}Yb, 14.31% ^{171}Yb ($I=\frac{1}{2}$), 21.82% ^{172}Yb, 16.13% ^{173}Yb ($I=\frac{5}{2}$), 31.84% ^{174}Yb, and 12.73% ^{176}Yb]. Similar broad lines and anomalous intensity ratios are also evident in the saturated absorption spectra reported for the Yb^+ 328.9-nm $6s$-$6p_{1/2}$ transition by Berends and Maleki [6].

The broad lines and anomalous intensity ratios can be interpreted in terms of the effects of velocity-changing collisions (VCC's), which can be very pronounced for transitions in ionized atoms such as Yb^+ on account of the long-range monopole-dipole interaction. Such VCC effects are particularly severe for systems in which there is strong branching out of the upper level into "reservoir" levels not coupled to the laser field [21]. Under these conditions, essentially all velocity groups in the ground state are coupled to the laser field by VCC's, and optically pumped into the reservoir levels. Thus, provided there is sufficient time between successive "on" times of the modulated laser pump beam for fresh atoms to diffuse into the laser interaction region, the signal recorded by the lock-in (which is the difference in transmission of the probe beam with the pump beam off and on) will exhibit large Doppler-broadened pedestals. In the case of the even isotopes, branching out of the laser-excited Yb^+ 369.4-nm transition is small, about 0.5% [22]. However, in the case of the odd isotopes, branching out of the laser-excited transition ranges from as high as 67% for hyperfine component 171c, which exhibits a very intense, broad saturated absorption line [Fig. 2(a)], to just 0.5% for component 171a, which exhibits a weak, narrow saturated absorption line similar to that of the even isotope components.

For the saturated absorption spectrum in Fig. 2(b), the modulation frequency of the laser pump beam was raised by a factor of 2, and the argon pressure in the discharge lowered by a factor of 2.5. In this case, diffusion of fresh Yb^+ ions into the laser interaction region during successive "on" times of the laser pump beam is reduced considerably, and the fraction of Yb^+ ions that are optically pumped into reservoir levels remains approximately constant throughout the modulation cycle. Under these conditions, the large VCC pedestals are subtracted out by the lock-in amplifier and narrow, Doppler-free saturated absorption spectra having approximately normal component intensities are observed [Fig. 2(b)]. In particular, the very intense, odd-isotope components observed in Fig. 2(a) are now reduced to about their expected intensities. The width of the even-isotope components in Fig. 2(b) is about 50 MHz (FWHM), which is to be compared with the natural linewidth of 19.9(5) MHz [23].

In the spectrum in Fig. 2(b), all isotope and hyperfine

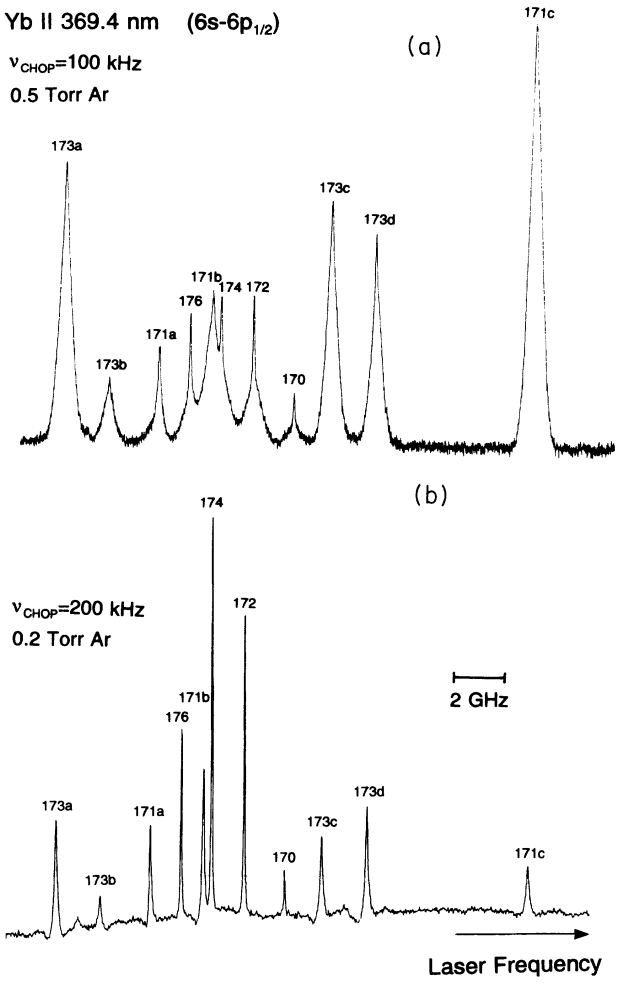

FIG. 2. Saturated absorption spectra for the Yb^+ 369.4-nm ($6s$-$6p_{1/2}$) transition, obtained using (a) a chopping frequency for the laser pump beam of 100 kHz, and a sputtering discharge at 0.5-Torr Ar; (b) a chopping frequency for the laser pump beam of 200 kHz, and a sputtering discharge at 0.2-Torr Ar.

components are clearly observed except for the very weak ^{168}Yb component (0.135%). The separations of the 171b and 171c, 173a and 173c, and 173b and 173d components are consistent with the accurately known 6*s* hyperfine splittings in $^{171}Yb^+$ and $^{173}Yb^+$ [10,12].

III. RESULTS

A. Hyperfine structures

The magnetic hyperfine interaction constants (*A* factors) for ^{171}Yb and ^{173}Yb deduced from the measured hyperfine splittings in 23 spectra similar to Fig. 2(b) are listed in Table I, along with the early Doppler-limited data of Krebs and Nelkowski [7] and Chaiko [9] and the accurate microwave-optical double-resonance results for the 6*s* state [10–12]. For completeness, hyperfine interaction constants for the Yb^+ $6p_{3/2}$ state are also included [6,24]. The quoted uncertainties in the present *A* factors represent two standard deviations in the mean plus a small contribution from the uncertainty in the frequency calibration (0.005%). Our *A* factors for the 6*s* ground state, which were obtained using the independently determined etalon calibration constant, 105.439(5) MHz, are in satisfactory agreement with the accurate microwave-optical double-resonance results [10,11], while our values for the $6p_{1/2}$ state represent a factor of 20–50 improvement in accuracy over the early Doppler-limited results [7,9].

Using the published value for the ratio of the nuclear magnetic moments $\mu_{173}/\mu_{171} = -1.377\,23(7)$ [25–28], our *A* factors for the $6p_{1/2}$ level lead to the following result for the hyperfine anomaly [29] of the $6p_{1/2}$ state in Yb^+:

$$\begin{aligned}\Delta_{171,173}(6p_{1/2}) &= [A_{171}/A_{173}][(\mu_{173}/I_{173})/(\mu_{171}/I_{171})]-1 \\ &= -0.0024(9)\,, \end{aligned} \tag{1}$$

where the uncertainty represents two standard deviations in the mean. The above result, together with the result $\Delta_{171,173}(6s) = -0.004\,240(5)$ deduced from the accurate *A* factors of Münch *et al.* [10] and Bauch, Schnier, and Tamm [12], yields the ratio $\Delta_{171,173}(6p_{1/2})/\Delta_{171,173}(6s) = 0.57(21)$. This result is to be compared with a ratio of about 0.2 obtained for numerically determined orbitals (Sec. IV B) and also from the analytical re-

TABLE I. Hyperfine interaction constants for levels in Yb^+. The *B* factors (in the case of the $6p_{3/2}$ state) are shown in square brackets. As discussed in Sec. IV, the $6p_{3/2}$ state is strongly perturbed, which makes the calculated *A* factors (shown in parentheses) very uncertain for this state.

	$A(^{171}\text{Yb},\ I=\frac{1}{2})$ (GHz)		$A(^{173}\text{Yb},\ I=\frac{5}{2})$ (GHz)	
	This work	Other work	This work	Other work
		6*s* state		
Expt.	12.645(2)	12.68[a]	−3.4975(6)	−3.508(9)[a]
		12.72(3)[b]		−3.50(1)[b]
		12.642 812 124 2(14)[c]		−3.497 240 079 85(3)[d]
		12.642 812 119 6(4)[e]		
		12.642 812 118 471(9)[f]		
MBPT[g]	12.73		−3.507	
		$6p_{1/2}$		
Expt.	2.1049(13)	2.16[a]	−0.5812(4)	−0.600(9)[a]
		2.13(3)[b]		−0.60(1)[b]
MBPT[g]	2.317		−0.638	
		$6p_{3/2}$		
Expt.		0.877(20)[g]		−0.245(10)[h]
				[B = 1.460(50)[h]]
				−0.255(30)[i]
				[B = 0.018(3)[i]]
MBPT[f]	{0.391}		{−0.107}	
			[B = 1.78]	

[a]Krebs and Nelkowski [7].
[b]Chaiko [9].
[c]Blatt, Schnatz, and Werth [56].
[d]Münch *et al.* [10].
[e]Casdorff *et al.* [11].
[f]Bauch *et al.* [12].
[g]Many-body perturbation theory calculations taken from Table IV, using the values $\mu_{171} = 0.493\,67(1)\mu_N$ and $\mu_{173} = -0.679\,89(3)\mu_N$ [28].
[h]Berends and Maleki [6].
[i]Krebs and Nelkowski [24].

sults of Stroke, Blin-Stoyle, and Jaccarino [30] for $Z=70$. The inclusion of many-body effects would be expected to raise this value, in particular the admixture of $6p4f \rightarrow 6s5d$ excitations.

B. Isotope shifts

The Yb^+ 369.4-nm $6s$-$6p_{1/2}$ isotope shifts determined from the center frequencies of the even-isotope components and from the centroids of the odd-isotope components are listed in Table II, along with early Doppler-limited results [7–9]. The quoted uncertainties represent two standard deviations in the mean plus a small contribution from the uncertainty in the frequency calibration (0.005%). The present isotope shift results for the 369.4-nm transition represent 1–2 orders of magnitude improvement in accuracy over the early Doppler-limited data [7–9]. Table II also includes isotope shifts reported for the Yb^+ 328.9-nm $6s$-$6p_{3/2}$ transition by Berends and Maleki [6], and for the neutral Yb 555.6-nm $6\,^1S_0$–$6\,^3P_1^o$ transition by Clark *et al.* [4].

The isotope shift between a pair of isotopes of masses M_{A_1} and M_{A_2} for a transition i can be expressed as the sum of mass shift and field shift components [5]:

$$\delta\nu_i=[(M_{A_2}-M_{A_1})/(M_{A_1}M_{A_2})]K_i+\delta\nu_1^{\mathrm{FS}} . \tag{2}$$

The mass shift component arises from the kinetic energy $\mathbf{p}_N^2/2M_A=(\sum_i \mathbf{p}_i^2+\sum_{i\neq j}\mathbf{p}_i\cdot\mathbf{p}_j)/2M_A$ of the nucleus with its finite mass M_A, where the first term leads to the normal mass shift (NMS), characterized by the constant $K^{\mathrm{NMS}}=m_e\nu_i$ (where $m_e=5.48580\times10^{-4}$ u, and ν_i is the transition frequency), and the second term gives the "mass polarization" or the specific mass shift, characterized by

$$K^{\mathrm{SMS}}=\langle\sum_{i\neq j}\mathbf{p}_i\cdot\mathbf{p}_j\rangle/h . \tag{3}$$

The field shift arises from differences in the nuclear charge distributions, leading to a slightly different nuclear potential for different isotopes, and is characterized by the constant

$$F_i=(2\pi/3)Ze^2\Delta|\Psi(0)|_i^2 , \tag{4}$$

where $\Delta|\Psi(0)|_i^2$ is the difference in electron density at the nucleus between the two electronic states. Since the electron density varies slightly within the nucleus, the experimental isotope shift is sensitive not only to the difference in mean-square charge radius between the nuclei of isotopes A_1 and A_2, $\delta\langle r^2\rangle^{A_1,A_2}$, but also to higher moments of the nuclear change distribution in a combination usually denoted by λ^{A_1,A_2}:

$$\delta\nu_i^{\mathrm{FS}}=F_i\lambda^{A_1,A_2} \tag{5a}$$

$$=F_i\delta\langle r^2\rangle^{A_1,A_2}[1+(c_2/c_1)\delta\langle r^4\rangle^{A_1,A_2}/\delta\langle r^2\rangle^{A_1,A_2}+(c_3/c_1)\delta\langle r^6\rangle^{A_1,A_2}/\delta\langle r^2\rangle^{A_1,A_2}+\cdots]$$

$$=F_i(1-\kappa)\delta\langle r^2\rangle^{A_1,A_2} . \tag{5b}$$

To take these higher moments into account, we have evaluated the expectation value of the difference in potential for two nuclei with slightly different Fermi charge distributions, as described in more detail by Hartley and Mårtensson-Pendrill [3]. For Yb we find that the higher moments give a reduction of about 5%, depending slightly on the parameters used in the Fermi distributions. This is in agreement with the value $\kappa=0.048$ given by Torbohm, Fricke, and Rosén [31].

Introducing the modified isotope shift, defined by

$$\xi_i=[M_{A_1}M_{A_2}/(M_{A_2}-M_{A_1})]\delta\nu_i , \tag{6}$$

then for a pair of transitions i,j, the above expressions (2), (5a), and (5b) lead to

$$\xi_i=(F_i/F_j)\xi_j+(K_i-K_jF_i/F_j) . \tag{7}$$

Thus a King plot [32] of ξ_i versus ξ_j should then yield a straight line of slope F_i/F_j and intercept $(K_i-K_jF_i/F_j)$, provided the electronic and nuclear factors F_i and λ^{A_1,A_2} are separable.

Figure 3 shows King plots of the isotope shift data for the Yb^+ 369.4-nm $6s$-$6p_{1/2}$ transition and the Yb^+ 328.9-nm $6s$-$6p_{3/2}$ transition (data of Berends and Maleki [6]) versus the accurate isotope shift data for the neutral

TABLE II. Isotope shifts (in GHz) for the Yb^+ 369.4-nm ($6s$-$6p_{1/2}$), Yb^+ 328.9-nm ($6s$-$6p_{3/2}$), and Yb I 555.6-nm ($6\,^1S_0$-$6\,^3P_1^o$) resonance lines.

		Yb^+ 369.4 nm				Yb^+ 328.9 nm	Yb 555.6 nm
A_1	A_2	This work	Ref. [7]	Ref. [8]	Ref. [9]	Ref. [6]	Ref. [4]
170	172	−1.623 3(8)	−1.499(90)	−1.661(39)	−1.640(3)	−1.459(21)	−1.286 47(50)
171	172	−1.034 3(8)			−1.142(30)	−0.920(15)	−0.825 77(50)
173	172	0.569 9(7)			0.516(30)	0.535(38)	0.444 56(50)
174	172	1.275 3(7)	−1.409(90)	1.277(48)	1.265(3)	1.154(11)	1.000 28(50)
176	172	2.492 8(10)	−2.698(130)	2.482(62)	2.470(3)	2.259(13)	1.955 04(50)

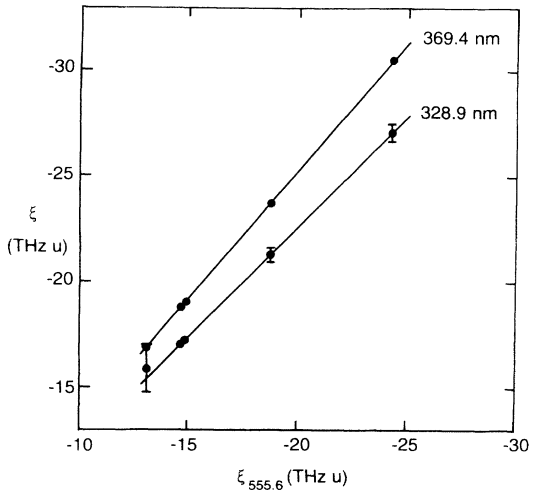

FIG. 3. King plots of the isotope shift data for the Yb^+ 369.4-nm ($6s$-$6p_{1/2}$) and Yb^+ 328.9-nm ($6s$-$6p_{3/2}$) transitions vs the isotope shift data for the Yb I 555.6-nm ($6\,^1S_0$-$6\,^3P_1^o$) transition. The isotope shift data for the Yb^+ 328.9-nm and Yb I 555.6-nm transitions were taken from Berends and Maleki [6] and Clark *et al.* [4], respectively. The error bars in the case of the Yb^+ 369.4-nm transition are smaller than the data points. The straight lines represent weighted least-squares fits to the data.

Yb 555.6-nm $6\,^1S_0-6\,^3P_1^o$ transition (data of Clark *et al.* [4]). The data points for the 369.4-nm transition all fall on the straight line within the quoted uncertainties, and this serves as a consistency check on the isotope shift data. In the case of the 328.9-nm transition, the differences from the straight line are much larger and reflect the larger uncertainties in those data. The slopes and intercepts determined from weighted least-squares fits to the King plots are listed in Table III.

IV. CALCULATIONS

In order to interpret the experimentally determined isotope shifts, electronic factors are needed, in particular for the field shift, but preferably also for the specific mass shift. In this work we have performed coupled-cluster calculations for the $6s$ and $6p$ states of Yb^+. The calculations of the wave functions are described in Sec. IV A. The resulting wave functions were then used to evaluate field shift constants F and hyperfine structure factors A and B, as described in Sec. IV B. The results are shown in Table IV. In addition, a less complete calculation of the specific mass isotope shift constants K^{SMS} is presented in Sec. IV D and Table V.

TABLE III. Slopes and intercepts of (weighted) King plots. The isotope shift data for the Yb I 555.6-nm and Yb^+ 328.9-nm transitions were taken from Clark *et al.* [4] and Berends and Maleki [6], respectively.

Transition		Slope	Intercept
1	2		(THz u)
Yb^+ 369.4 nm	Yb I 555.6 nm	1.216(3)	−0.88(5)
Yb^+ 328.9 nm	Yb^+ 369.4 nm	0.863(17)	−0.81(34)

A. The coupled-cluster approach

A fully relativistic Dirac-Fock (DF) calculation, in which orbitals are obtained in the potential from the unperturbed Yb^{2+} core, is taken as the starting point. Strong evidence for relativistic effects is found from the hyperfine structure and from the field shift, both of which are sensitive to the wave function close to the nucleus: in a nonrelativistic central-field model the ratio between the calculated magnetic hyperfine interaction constants for the $6p_{3/2}$ and $6p_{1/2}$ states is 0.2, which is to be compared with the smaller ratio 0.12 obtained for the DF values, as seen in Table IV. This is explained by the relativistic correction factors for the hyperfine structure, tabulated by Kopfermann [33]. For $Z=70$ they amount to 1.7837 and 1.1116 for $j=\frac{1}{2}$ and $\frac{3}{2}$ states, respectively. The field shift is even more sensitive to relativistic effects: the expression for this correction factor obtained by Bauche [34] gives 5.17 for $Z=70$.

The corrections of the core due to the presence of the valence electron, as well as the correlations among the core electrons and their effect on the valence electron, are accounted for by using many-body perturbation theory in the coupled-cluster approach [15]. Single excitations, which correspond to modification of the occupied orbitals to approximate Brueckner orbitals, and double excitations, which lead to "pair functions," were included. The exact wave function is then approximated by an exponential of single and double excitation clusters acting on the unperturbed wave function. The excitations are described in terms of a numerical basis set obtained by diagonalizing the unperturbed Hamiltonian, as described by Salomonson and Oster [35]. A grid with 71 points in the range $\exp(-6.5)/Z$ to $\exp(8.7)/Z$ (in atomic units a_0) was used.

After the basis set was obtained, the excitations from the closed-shell core of Yb^{2+} were first evaluated, including six coupled iterations of pair excitations from $4p^2$ and up. For the $4f^2$ excitations, six additional iterations were then performed. This wave function for the core was then used as a starting point to evaluate pair excitations from the valence orbital combined with a core orbital from $4s$ or higher. For the more important pairs, terms up to $k=4$ were kept in the multipole expansion of the electron-electron interaction, $1/r_{12}$, whereas excitations up to $k=2$ or 3 were kept for the less important pairs. For the $6s$ and $6p_{1/2}$ states, 11 iterations were performed and found to give stable results for the properties evaluated, whereas the $6p_{3/2}$ results converge considerably more slowly. The $6p_{3/2}$ results shown in Table IV were obtained after 14 iterations and are discussed in more detail below.

The energy eigenvalues obtained in these coupled-cluster calculations are $\varepsilon_{6s}=-0.4489$ a.u., $\varepsilon_{6p_{1/2}}=-0.3219$ a.u., and $\varepsilon_{6p_{3/2}}=-0.3062$ a.u., compared with the experimental values $\varepsilon_{6s}=-0.4477$ a.u.,

TABLE IV. Calculated hyperfine-structure constants A/g_I (GHzμ_N^{-1}), B/Q (GHz b^{-1}), and electronic field shift constants F (GHz fm^{-2}) for the 6s and 6p states of Yb^+. The A/g_I and F factors for the strongly perturbed $6p_{3/2}$ state are very uncertain (Sec. IV), and are shown in parentheses. A detailed description of the various contributions is given in Ref. [57].

	$6s$		$6p_{1/2}$		$6p_{3/2}$		
	A_{6s}/g_I	F_{6s}	$A_{6p_{1/2}}/g_I$	$F_{6p_{1/2}}$	$A_{6p_{3/2}}/g_I$	$F_{6p_{3/2}}$	$B_{6p_{3/2}}/Q$
DF[a]	9.791	−11.97	1.562	−0.365	0.184	0	0.373
BO[b]	2.664	−3.25	0.611	−0.143	0.067	0	0.136
RPA (1st)[c]	0.911	−0.86	0.256	0.047	0.056	0.137	0.157
RPA-it[d]	−0.002	−0.45	0.002	−0.298	0.001	−0.211	−0.002
Corr[e]	−0.089	0.12	0.002	−0.299	0.102	−0.345	−0.007
Norm[f]	−0.380	0.47	−0.086	−0.037	−0.014	0.014	−0.023
Total	12.894	−15.94	2.347	−1.021	(0.396)	(−0.405)	0.635

[a]Dirac-Fock contribution.
[b]Brueckner orbital contribution.
[c]Random-phase-approximation corrections—first order.
[d]RPA corrections—iterated.
[e]Remaining correlation effects.
[f]Accounts for normalization of wave functions.

$\varepsilon_{6p_{1/2}} = -0.3244$ a.u., and $\varepsilon_{6p_{3/2}} = -0.3093$ a.u. [36]. The numbers imply only a slight improvement over the second-order energy values $\varepsilon_{6s} = -0.4682$ a.u., $\varepsilon_{6p_{1/2}} = -0.3277$ a.u., and $\varepsilon_{6p_{3/2}} = -0.3135$ a.u., obtained by Koc and Migdalek [37], and their values obtained by adding an approximate "core polarization potential" to the DF equations $\varepsilon_{6s} = -0.4343$ a.u., $\varepsilon_{6p_{1/2}} = -0.3133$ a.u., and $\varepsilon_{6p_{3/2}} = -0.2991$ a.u. Our value for the 6p fine-structure splitting, 0.0157 a.u., is about 3% larger than the experimental value 0.0152 a.u. [36]. Better agreement is found by Fawcett and Wilson [38], who use a pseudorelativistic Hartree-Fock approach and fit Slater integrals and some of the spin-orbit parameters using experimental data. Their estimate of the 6p fine structure, for example, is 0.0151 a.u.

Both of the 6p states are strongly mixed with the $4f^{13}5d6s$ configuration (and to some extent with $4f^{13}5d^2$). Fawcett and Wilson [38] find that the admixture is about 20% in $6p_{1/2}$, but approaching 40% for the $6p_{3/2}$ state, which actually lies above the lowest $J=\frac{3}{2}$ state [with the designation $^2F_{7/2}\,^3D_{3/2}$ in the *LSJ LKJ* coupling—see Fig. 1(a)] of the $4f^{13}5d6s$ configuration. This configuration is described by the pair excitations $6p4f \rightarrow ds$ and $6p4f \rightarrow sd$, for which several additional iterations were performed. This is a classical "intruder problem" [39], and it is hardly surprising that the perturbation expansion converges very slowly, if at all. The problem may be further aggravated by the asymmetric handling of occupied and intermediate states, inherent in the intermediate normalization formulation of the coupled-cluster approach [40], and it is likely that an extended model space formulation [41] would be necessary to obtain an adequate description of the $6p_{3/2}$ state. The theoretical results quoted in Tables IV and V for the $6p_{3/2}$ state are thus very uncertain.

TABLE V. Contributions to the calculated SMS constant K^{SMS} (in THz u), for the 6s and 6p states in Yb^+ with respect to the core of Yb^{2+}.

	$6s$	$6p_{1/2}$	$6p_{3/2}$
	DF		
1st order	−2.305	−1.068	−0.739
RPA	1.643	0.798	0.762
Corr	0.903	0.237	0.188
	BO corrections		
1st order	−0.296	−0.277	−0.174
RPA	0.244	0.190	0.164
Corr	0.217	0.076	0.050
Total	0.405	−0.043	−0.251

B. Field shift and hyperfine structure

As discussed in Sec. III B, the field isotope shift is determined by the difference in electron density at the nucleus between the two electronic states, and the electronic factor for the FS can be obtained from expectation values of the perturbation:

$$h^{FS} = -(Z/6)\delta(r)/r^2 \,. \tag{8}$$

In many-body perturbation theory, the electronic factors are obtained directly with respect to the unperturbed core of Yb^{2+}, and include only the contributions due to the *change* in the core induced by the 6s or 6p valence electron [42].

Like the field isotope shift, the hyperfine structure for an s state is determined by a contact interaction in the nonrelativistic case. A direct comparison between the expressions for the FS and the contact hyperfine interaction leads to a nonrelativistic ratio $F_{ns}/(A_{ns}/g_I) = -0.431\mu_N\,\text{fm}^{-2}$ (μ_N is the nuclear magneton) for $Z=70$ [1]. In the relativistic formulation, used in the present work, the magnetic hyperfine interaction is in-

stead described by

$$h^{\mathrm{mhfs}} = c\boldsymbol{\alpha}\cdot\mathbf{A} = -ic(\mu_0/4\pi)[\boldsymbol{\alpha}\cdot(\boldsymbol{l}\mathbf{C}^1)]\cdot\boldsymbol{\mu}_I/r^2 , \quad (9)$$

where l is the orbital angular momentum and $\mathbf{A}$ is the vector potential from a point dipole μ_I. This operator does not have the same relativistic correction factors as the FS, leading to an increased ratio $F_{ns}/(A_{ns}/g_I) = -1.22\mu_N\,\mathrm{fm}^{-2}$ for the Dirac-Fock values.

The results given in Table IV were obtained with a nuclear magnetization distributed on a spherical shell at the nuclear radius. This changes the radial part of expression (9) for the interaction from l/r^2 to r/r_N^3 inside the nucleus, and was found to give a reduction of about 1% for A_{6s} and about 0.2% for $A_{6p_{1/2}}$, compared with the results for a point nucleus. For $A_{6p_{3/2}}$ the difference from a point nucleus is hardly noticeable.

For $j > \frac{1}{2}$, a nuclear electric quadrupole moment may contribute to the hyperfine structure through the interaction

$$h^{\mathrm{ehfs}} = -(e^2/8\pi\varepsilon_0)(1/r^3)\mathbf{C}^2\cdot\mathbf{Q} , \quad (10)$$

and in the last column in Table IV we give the calculated values of the electric quadrupole interaction constant B in terms of the nuclear quadrupole moment, Q.

1. The 6s state

The valence orbital expectation value accounts for about 75% of the final result both for the hyperfine structure and the field isotope shift constant. The dominant correlation contribution can be described by a modification of the valence orbital to an approximate Brueckner orbital, denoted by "BO" in Tables IV and V. The correlation effects make the valence orbital more tightly bound, increasing its probability at the nucleus and giving the same relative increase for both hyperfine structure and field isotope shift, about 27% of the DF value in this case, leaving relatively small contributions to be accounted for by the remaining terms. The random-phase approximation (RPA) terms describe the modification of the core orbitals due to the presence of the valence orbital. The contributions are different for the two properties, since only the "exchange diagrams" contribute for the hyperfine interaction which involves the nuclear spin, whereas the FS is described by a scalar operator and both direct and exchange terms enter. These diagrams account for the "spin polarization" in the case of the hyperfine interaction, and for the "screening" effects in the case of the field shift, but also include some correlation effects since they are evaluated with correlated wave functions. They give an increase of about 11% of the DF value for the field shift, and 9% for the hyperfine structure. The situation is very different from, for example, Ba^+, where the RPA terms made only a very small contribution to the field shift [2]. The remaining correlation contributions also differ between the two operators, but give only about 1% in both cases. As seen from Table I, the calculated hyperfine constants are within 0.7% of the experimental values. This result has been found to change very little with continued iterations. Since the DF and BO terms, which contribute in the same way to both the hyperfine constant and the field shift, account for a large fraction of the final result, the uncertainty in F_{6s} should be of the same order, giving us a final result, $F_{6s} = -15.94(16)\ \mathrm{GHz\,fm}^{-2}$.

2. The $6p_{1/2}$ state

The small component of a relativistic $p_{1/2}$ orbital gives it a finite probability density at the origin. In the case of Ba^+, this accounts for essentially all the difference between the F values for the $6p_{1/2}$ and $6p_{3/2}$ states—the remaining contributions are nearly identical [2,43]. We note that for Ba^+, the field shift constants for both p states were positive, due to large RPA contributions. In the case of Yb^+, RPA contributions are fairly modest, with larger negative contributions both from the higher-order RPA terms and from correlation effects. With many comparable contributions it is difficult to assess the accuracy. The calculated hyperfine constants are about 10% larger than the experimental values (Table I), but have a very small correlation contribution, apart from the BO correction which gives a 39% increase over the DF value. The results in Table IV were obtained after 11 iterations, and seem to be relatively stable: after four iterations, the hyperfine constant was only 2% smaller than that given in Table IV. The field shift constant was $-0.84\ \mathrm{GHz\,fm}^{-2}$ after four iterations, and changed to $-1.00\ \mathrm{GHz\,fm}^{-2}$ after a further four iterations, with changes mainly in the RPA and in the correlation terms. The result thus seems sufficiently converged, and residual errors should be due to omitted excitations.

From the calculated factors for F_{6s} and $F_{6p_{1/2}}$, we obtain $F_{6s\text{-}6p_{1/2}} = -14.9(2)\ \mathrm{GHz\,fm}^{-2}$, where the quoted uncertainty includes a reasonable estimate ($\pm 10\%$) of the error in $F_{6p_{1/2}}$. This value is larger than the result $F_{6s\text{-}6p_{1/2}} = -12.94\ \mathrm{GHz\,fm}^{-2}$ obtained by Torbohm, Fricke, and Rosén [31] in a DF calculation, but somewhat smaller than semiempirical estimates [31], around $-17.2\ \mathrm{GHz\,fm}^{-2}$ [using updated values for the function $f(Z)$ tabulated by Aufmuth, Heilig, and Steudel [5]], consistent with the trend observed in earlier calculations [2].

The factor, $F_{6s\text{-}6p_{1/2}} = -14.9(2)\ \mathrm{GHz\,fm}^{-2}$, calculated for Yb^+, can now be used together with the slopes of King plot data to deduce F_i factors for any transition in Yb for which isotope shift data are available. For example, when combined with the slopes of the King plots given in Table III, we obtain $F = -12.9(3)\ \mathrm{GHz\,fm}^{-2}$ for the Yb^+ $6s\text{-}6p_{3/2}$ transition, and $F = -12.3(2)\ \mathrm{GHz\,fm}^{-2}$ for the Yb I $6\,{}^1S_0\text{-}6\,{}^3P_1^o$ transition.

3. The $6p_{3/2}$ state

A $p_{3/2}$ orbital, like a nonrelativistic p orbital, has no probability density at the origin. Still, it gives a small contribution (of the order $-8\ \mathrm{kHz\,fm}^{-2}$ for $6p_{3/2}$ in Yb^+) to the field isotope shift through the higher moments of the nuclear charge distribution. This contribution is, of course, negligible compared with those resulting from the perturbation of the core electrons. For the

hyperfine structure, a $p_{3/2}$ orbital contributes to the A factor through "orbital" and "spin-dipole" interactions in the nonrelativistic case and the DF value gives nearly half of the final result. This situation makes the FS particularly sensitive to changes in the wave function. As discussed above, the $6p_{3/2}$ state is very perturbed, due to strong mixing with the $(4f^{13})_{7/2}6s5d$ configuration—one of the $J=\frac{3}{2}$ states resulting from this configuration lies below the $6p_{3/2}$ state, making the situation very different from the $6p_{1/2}$ case. In the results shown in Table IV, the Brueckner orbital contribution amounts to about 36% of the DF value, both for electric quadrupole and magnetic hyperfine structures, and is comparable with that for the $6p_{1/2}$ state. The RPA contributions are two to three times larger than for $6p_{1/2}$ and, whereas the correlation contribution to $A_{6p_{1/2}}$ is negligible, it amounts to more than half of the DF value for $A_{6p_{3/2}}$.

The perturbed character of the $6p_{3/2}$ state is also apparent in the calculations, e.g., from the large changes in the values with further iterations, in particular for the field shift constant. The situation is thus very different from that of the $6p_{1/2}$ state, as discussed above. The value of $F_{6p_{3/2}}$ was found to be -0.16 GHz fm^{-2} after six iterations, -0.25 GHz fm^{-2} after ten iterations, and -0.40_5 GHz fm^{-2} after 14 iterations. Thus there is no sign of convergence for $F_{6p_{3/2}}$, and so this result is shown in parenthesis in Table IV. Comparison of the calculated $F_{6p_{3/2}}$ value with that deduced from the measured slope $(F_{6s\text{-}6p_{3/2}}/F_{6s\text{-}6p_{1/2}})$ of the King plot of 328.9 nm versus 369.4 nm (Table III) and from the calculated values of F_{6s} and $F_{6p_{1/2}}$ suggests that the calculated $F_{6p_{3/2}}$ (after 14 iterations) is underestimated by a factor of about 8. For the hyperfine structure, the result for A/g_I was 0.35 GHz μ_N^{-1} after six iterations, 0.38 GHz μ_N^{-1} after ten iterations, and 0.396 GHz μ_N^{-1} after 14 iterations (as in Table IV). Comparison of the calculated magnetic hyperfine A factors with the experimental A factors (Table I) indicates that the calculated factors are underestimated by a factor of about 2.2. For the $6p_{3/2}$ state, we have also evaluated the contributions to the electric quadrupole interaction constant, which was found to be much less sensitive to correlation effects. The result after six and ten iterations is $B/Q=0.634$ and 0.636 GHz b^{-1}, respectively, very close to the result in Table IV. The calculated electric quadrupole B factor, deduced assuming a value of $Q(^{173}\text{Yb})=2.80(4)$ b [45], is within about 20% of the latest experimental value [6] (Table I).

To investigate further the sensitivity to correlation effects, we evaluated the properties omitting various pair excitations: for example, inclusion of only core-valence pair functions (i.e., omitting all core-core excitations) gives small differences in the various contributions—although the RPA terms for the FS are changed from 0.14 to 0.18 GHz fm^{-2}—and of course the iterated RPA-like terms, which are constructed using core-core pair functions, vanish. These give significant contributions only for the field shift. As a next step we performed additional iterations for the outer core-core pair functions, which were found to have a very small effect on the results. We then evaluated the remaining core-valence excitations, down to $6p1s$, performing four iterations of these pair excitations and including terms up to $k=2$ in the multipole expansion. This changed mainly the RPA-like contributions. The change is particularly drastic for the field shift, where the RPA contributions changed from 0.14 to 0.18 GHz fm^{-2}. The total results were changed from the values in Table IV, leaving $A/g_I=0.406$ GHz μ_N^{-1}, $F=-0.217$ GHz fm^{-2}, and $B/Q=0.656$ GHz b^{-1}. Three further iterations of the outer core-valence pair functions, followed by ten iterations of the $6p4f$ excitations, changed these results to $A/g_I=0.424$ GHz μ_N^{-1}, $F=-0.286$ GHz fm^{-2}, and $B/Q=0.654$ GHz b^{-1}, where the last five iterations added about 1% to the A factor, 6% to F, and 0.1% to B. There is thus some indication of convergence, but very slow. It does, however, seem that further iteration of the pair excitations will be insufficient to bring the A factor close to the experimental value.

The reason for the failure is almost certainly due to an incorrect description of the $6p4f$ excitations, as discussed in Sec. IV A. These pair functions alone give a FS contribution of about the same size as the final result. Obviously the admixture of the s orbital in the $6p4f\rightarrow sd$ excitations leads to a significantly increased electron density at the nucleus. It also makes important contributions to the hyperfine structure, accounting for essentially all the correlation contribution (the smaller contributions from the other excitations essentially cancel each other). It is likely that the admixture of $6p4f\rightarrow 6s5d$ is severely underestimated by perturbation theory.

C. Transition matrix elements

As an additional check, the coupled-cluster wave functions obtained as described above were used to evaluate reduced transition matrix elements $\langle 6s\|er\|6p_j\rangle$, and hence lifetimes, for the $6p$ states assuming a negligible transition probability for the transitions to the metastable $5d$ states [38]. The transition matrix element is sensitive to details of the radial wave function at larger distances from the nucleus than the electronic FS or the hyperfine interaction constants, and it is also much less sensitive to correlation effects.

Our calculated lifetime values, $\tau(6p_{1/2})=7.0$ ns and $\tau(6p_{3/2})=5.0$ ns, which have recently been reported in a separate paper [23], are 10–20% shorter than the latest experimental values $\tau(6p_{1/2})=8.0(2)$ ns and $\tau(6p_{3/2})=6.3(3)$ ns, obtained by laser-induced fluorescence [23], and $\tau(6p_{1/2})=8.10(13)$ ns obtained by the beam laser technique [46]. Differences between the theoretical and experimental results are likely to result from an underestimation of the $4p4f\rightarrow 6s5d$ admixture, especially for the $6p_{3/2}$ state, as discussed in Sec. IV B.

D. The specific mass shift

The specific mass shift describes a correlation of electronic momenta arising through the motion of the nu-

cleus with its finite mass. The proper treatment of nuclear recoil in the relativistic case is still an unsolved problem, and here we use the nonrelativistic operator Eq. (3), although the orbitals are obtained relativistically.

The first contribution to K^{SMS} is the interaction of the valence electron with all core electrons, i.e., those core orbitals whose l-quantum number differs by one unit and whose j-quantum number differs by at most one unit from the values for the valence electron. This result is given in the first line (denoted DF) of Table V. Only the exchange terms contribute, making this contribution negative. Of course the interaction also affects the core electrons, and even if we omit the enormous expectation value arising from their interaction we have to take into account the change it causes in the wave function for the core and hence in its interaction with the valence electron. This leads to the contribution denoted "RPA" in Table V, and cancels a large part of the DF contribution. Bauche [47], in his pioneering nonrelativistic isotope shift calculations, included not only the core electrons, as done in the present work, but also the valence electron(s) in the Hartree-Fock potential. These calculations then include automatically also the RPA terms. Being a two-particle operator, the SMS is very sensitive to correlation effects, which arise already in second order, giving results denoted by "Corr" in Table V. These contributions were evaluated by direct summation of the numerical spectrum, obtained using the methods described by Salomonson and Öster [35].

The modification of the valence orbital to an approximate Brueckner orbital is often the most important correlation effect, as seen, for example, in the calculations of hyperfine structure and field shift described in Sec. IV B. In the SMS calculation, we evaluated these corrections to lowest order, leading to an increase by about 15–25 % of all the contributions described above. These modifications are shown in the lower part of Table V. The calculations are essentially analogous to those by Hartley and Mårtensson-Pendrill [3] for Cs and Tl, although in the present calculations we have not included the effect of the SMS interaction on the excited orbitals, which was found to give quite small contributions in Cs. Work is in progress to evaluate SMS constants using full coupled-cluster wave functions. The correlation effects are sufficiently large to make both the $6s$ and $6p_{3/2}$ SMS constants positive, leaving the $6p_{1/2}$ constant close to zero.

The calculated SMS cannot be compared directly with experimental results, but we can compare a combination of the isotope shift factors of the two transitions obtained from the slope and intercept in a King plot: $K_{6s\text{-}6p_{3/2}}-\rho K_{6s\text{-}6p_{1/2}}$, where $\rho=0.863(17)$ is the slope obtained from the King plot of the isotope shift data of the 328.9-nm $6s$-$6p_{1/2}$ transition against the isotope shift data of the 369.4-nm $6s$-$6p_{1/2}$ transition (Table III). The calculated SMS constants lead to an intercept -0.24 THz u, compared with the experimental value $-0.93(34)$ THz u (obtained after subtracting the NMS contribution of 0.118 THz u from the intercept in the last row of Table III), and the Dirac-Fock value for this combination is actually better than the final theoretical value. However, as discussed above, the $6p_{3/2}$ state is very strongly perturbed, and in the analysis of the isotope shifts in Sec. V A we use the result for the $6s$-$6p_{1/2}$ transition only. The calculated SMS constants for this transition, $K^{\mathrm{SMS}}_{6s\text{-}6p_{1/2}}=0.448$ THz u, is very close to the normal mass shift, $K^{\mathrm{NMS}}_{6s\text{-}6p_{1/2}}=0.445$ THz u, and for the extraction of the nuclear charge distribution parameter λ^{A_1,A_2} we use $K^{\mathrm{SMS}}_{6s\text{-}6p_{1/2}}=(1\pm1)K^{\mathrm{NMS}}_{6s\text{-}6p_{1/2}}$.

V. NUCLEAR CHARGE RADIAL PARAMETERS

A. Optical data

The nuclear charge distribution parameters λ^{A_1,A_2} and $\delta\langle r^2\rangle^{A_1,A_2}$ were extracted from the 369.4-nm $6s$-$6p_{1/2}$ isotope shift data using the calculated factors $F_{369}=-14.9(2)$ GHz fm^{-2}, $K^{\mathrm{SMS}}_{369}=(1\pm1)K^{\mathrm{NMS}}_{369}$, and $\kappa=0.048$ [31] in Eqs. (2), (5a), and (5b). The results are listed in Table VI along with previous results deduced from optical isotope shift data. The uncertainties in our λ^{A_1,A_2} values arise mainly from the uncertainties in the calculated K^{SMS}_{369} and F_{369} factors. Table VI also lists λ^{A_1,A_2} values for isotope pairs involving the rare isotope ^{168}Yb (0.135%) and the long chain of neutron-deficient radioactive isotopes $^{152,154,156-158,160-167,169}$Yb. These were determined from the Yb I 555.6-nm isotope shift data of Clark *et al.* [4], Buchinger *et al.* [16], Sprouse *et al.* [17], and Billowes [18], using the factors $F_{556}=-12.3(2)$ GHz fm^{-2} and $K^{\mathrm{SMS}}_{556}=1.2(4)$ THz u $=(4\pm1)K^{\mathrm{NMS}}_{556}$, which were derived from our calculated F_{369} and K^{SMS}_{369} factors and the King plot results in Table III. Our λ^{A_1,A_2} values are systematically lower by about 20% than the values reported by Clark *et al.* [4], and just within the uncertainties of the results tabulated by Aufmuth, Heilig, and Steudel [5].

The λ^{A_1,A_2} values of Clark *et al.* [4] were derived from their Yb I 555.6-nm ($6\,^1S_0-6\,^3P^o_1$) isotope shift data using a semiempirical estimate of the FS constant, $F_{556}=-11.5$ GHz fm^{-2}, and normalizing the results to λ^{A_1,A_2} values deduced from (uncorrected) muonic-atom and electronic x-ray isotope shift data (see Table VII). The FS constant F_{556} was determined from Eq. (4) using a value of $|\Psi(0)|^2_{6s}$ calculated from the Goudsmit-Fermi-Segre (GFS) formula together with a value of the screening ratio, $\gamma=\Delta|\Psi(0)|^2_{6s^2\text{-}6s6p}/|\Psi(0)|^2_{6s}=0.72$, obtained from Hartree-Fock (HF) calculations. The normalization to the (uncorrected) muonic-atom and x-ray isotope shift results is equivalent to choosing a SMS constant of $K^{\mathrm{SMS}}_{556}\approx 14K^{\mathrm{NMS}}_{556}$, which is much larger than the value, $K^{\mathrm{SMS}}_{556}=(4\pm1)K^{\mathrm{NMS}}_{556}$, derived from our calculated F_{369} and K^{SMS}_{369} factors and the King plot data in Table III. This is the major reason for the higher λ^{A_1,A_2} values of Clark *et al.*

The λ^{A_1,A_2} values of Aufmuth, Heilig, and Steudel [5] were determined from the Yb I 555.6-nm isotope shift data of Clark *et al.* [4] and Buchinger *et al* [16] using the result $\lambda^{174,176}=0.081(4)$ fm^2, which is a mean of three estimates. The first estimate, $\lambda^{174,176}=0.0852$ fm^2, was de-

TABLE VI. Nuclear charge distribution parameters, λ^{A_1,A_2} and $\delta\langle r^2\rangle^{A_1,A_2}$, for isotopes of Yb. The set of $\delta\langle r^2\rangle^{A_1,A_2}$ values were derived from the λ^{A_1,A_2} values using the relationship $\delta\langle r^2\rangle^{A_1,A_2}=\lambda^{A_1,A_2}/0.952$ [31]. The values of λ^{A_1,A_2} and $\delta\langle r^2\rangle^{A_1,A_2}$ for which $A_1<170$ were deduced from the Yb I 555.6-nm isotope shift data of previous workers [4,16–18] using the factors $F_{556}=-12.3(2)$ GHz fm^{-2} and $K_{556}^{SMS}=1.2(4)$ THz u$=(4\pm1)K_{556}^{NMS}$ found in this work (Sec. V A).

A_1	A_2	This work $\delta\langle r^2\rangle^{A_1,A_2}$ (fm^2)	This work λ^{A_1,A_2} (fm^2)	Clark *et al.* [4] λ^{A_1,A_2} (fm^2)	Aufmuth, Heilig, and Steudel [5] λ^{A_1,A_2} (fm^2)
174	176	0.090(2)	0.086(2)	0.109(8)	0.081(4)[a]
173	176	0.142(3)	0.135(3)	0.170(12)	0.127(7)[a]
172	176	0.184(5)	0.175(5)	0.223(16)	0.165(9)[a]
171	176	0.259(6)	0.247(6)	0.308(20)	0.234(12)[a]
170	176	0.303(7)	0.288(7)	0.362(24)	0.273(14)[a]
169	176	0.372(12)[b]	0.354(11)[b]		0.337(18)[b]
168	176	0.428(13)[a]	0.408(12)[a]		0.388(20)[a]
167	176	0.497(15)[b]	0.473(14)[b]		0.451(24)[b]
166	176	0.577(17)[b]	0.549(16)[b]		0.525(28)[b]
165	176	0.683(19)[b]	0.650(18)[b]		0.624(33)[b]
164	176	0.761(21)[b]	0.724(20)[b]		0.696(37)[b]
163	176	0.887(23)[b]	0.844(22)[b]		0.814(44)[b]
162	176	0.973(25)[b]	0.927(24)[b]		0.894(48)[b]
161	176	1.111(27)[b]	1.058(26)[b]		1.024(56)[b]
160	176	1.201(29)[b]	1.143(28)[b]		1.107(60)[b]
158	176	1.435(35)[b]	1.366(33)[b]		1.326(73)[b]
157	176	1.560(39)[c]	1.485(37)[c]		
156	176	1.670(39)[d]	1.590(37)[d]		1.548(78)[e]
154	176	1.944(45)[d]	1.850(43)[d]		
152	176	2.301(50)[d]	2.190(48)[d]		

[a]Using Yb I 555.6-nm isotope shift data of Clark *et al.* [4].
[b]Using Yb I 555.6-nm isotope shift data of Buchinger *et al.* [16].
[c]Using Yb I 555.6-nm isotope shift data of Billowes [18].
[d]Using Yb I 555.6-nm isotope shift data of Sprouse *et al.* [17].
[e]Using Yb I 769.9-nm isotope shift data of Buchinger *et al.* [16].

duced from the 555.6-nm 174-176 isotope shift of Clark *et al.*, with $F_{556}=-11.2$ GHz fm^{-2} and assuming $K_{556}^{SMS}=0$. The F_{556} factor was calculated from Eq. (4) using a value of $|\Psi(0)|^2_{6s6p}$ determined from the known hyperfine splitting in the Yb I $6s6p\ ^3P_1^o$ level together with a value of the screening ratio, $\gamma'=\Delta|\Psi(0)|^2_{6s^2\text{-}6s6p}/|\Psi(0)|^2_{6s6p}=0.95$, obtained from HF calculations. The second estimate, $\lambda^{174,176}=0.0785$ fm^2, was obtained in the same way as above, but with $F_{556}=-12.4$ GHz fm^{-2}. This F_{556} factor is a mean of values calculated from Eq. (4) using values of $|\Psi(0)|^2_{6s}$ determined from the known fine structure splitting of the Yb^+ $6p$ states (GFS formula) and from the known hyperfine splitting in the Yb^+ $6s$ state together with a

TABLE VII. Comparison of values for the nuclear charge distribution parameter λ^{A_1,A_2} (in fm^2) deduced from optical, electronic x-ray, and muonic-atom isotope shifts in Yb.

A_1	A_2	Optical This work	Electronic x-ray Ref. [50]	Muonic atom[a] Refs. [48,4]	Muonic atom (corrected)[b]
174	176	0.086(2)	0.103(12)	0.102(4)	0.068
172	174	0.090(2)	0.141(13)	0.114(3)	0.086
170	172	0.113(3)	0.163(19)	0.138(5)	0.128
173	174	0.049(1)	0.091(33)	0.066(5)	0.052
171	172	0.071(1)	0.086(14)	0.075(5)	0.070
170	171	0.042(1)	0.077(32)		
172	173	0.040(1)	0.050(27)		

[a]Assuming a Fermi charge distribution [Eq. (13)] with $\delta t^{A_1,A_2}=0$.
[b]Including approximate correction for nuclear deformation, using Eqs. (16) and (17) with $c=6.37$ fm, $t_0=2.3$ fm, and values of $\delta\beta$ and β estimated from the optical isotope shift data (Fig. 5).

value of the screening ratio, $\gamma=\Delta|\Psi(0)|^2_{6s^2\text{-}6s6p}/|\Psi(0)|^2_{6s}=0.78$, obtained from HF calculations. The third estimate, $\lambda^{174,176}=0.079$ fm^2, was deduced from the 174-176 isotope shift for the Yb^+ $6s\,^2S_{1/2}$-$5d\,^2D_{3/2}$ $E2$ transition, with $F_{435}=-21.1$ GHz fm^{-2} and assuming $K^{\rm SMS}_{6s\text{-}5d}=1.4\pm0.9$ THz u$=(3.6\pm2.4)K^{\rm NMS}_{6s\text{-}5d}$. This $F_{6s\text{-}5d}$ factor is also the mean of values calculated from Eq. (4) using values of $|\Psi(0)|^2_{6s}$ determined from the known fine-structure splitting of the Yb^+ $6p$ states and from the known hyperfine splitting in the Yb^+ $6s$ state together with a screening ratio, $\beta'=\Delta|\Psi(0)|^2_{6s\text{-}5d}/|\Psi(0)|^2_{6s}=1.33$, obtained from HF calculations. The level of agreement between the λ^{A_1,A_2} values of Aufmuth, Heilig, and Steudel and those of the present work is to some extent fortuitous: in the Yb I 555.6-nm analysis of Aufmuth, Heilig, and Steudel, the use of a smaller F_{556} factor partly compensates for the effect of the smaller $K^{\rm SMS}_{556}$ $(=0)$ factor. The procedure of Aufmuth, Heilig, and Steudel has recently been used in the analysis of the isotope shift data for the long chain of radioactive Yb isotopes by Sprouse *et al.* [17] and Billowes [18].

B. Comparison of optical data with muonic-atom and x-ray data

In Table VII the λ^{A_1,A_2} values deduced from our optical isotope shift data are compared with values derived from muonic-atom isotope shifts [44,48] and electronic x-ray isotope shifts [49,50]. The muonic-atom and electronic x-ray λ^{A_1,A_2} values are systematically higher than the optical values: the ratio of muonic-atom to optical values ranges from 1.06 ± 0.08 (^{171}Yb-^{172}Yb) to 1.35 ± 0.12 (^{173}Yb-^{174}Yb), while the ratio of electronic x-ray to optical values varies from 1.20 ± 0.14 to 1.9 ± 0.7.

For muonic atoms, there is no specific mass shift, and the λ^{A_1,A_2} and $\delta\langle r^2\rangle^{A_1,A_2}$ factors derived from the FS depend on the nuclear charge model assumed in the analysis [48]. The usual method for analyzing muonic-atom isotope shifts is to use a model-independent analysis, in which the muonic-atom FS is expressed as [4,48]

$$\delta E^{\rm FS}=B_Z\delta\langle r^k e^{-\alpha r}\rangle^{A_1,A_2}=C_Z^{-1}\delta R_k\ , \tag{11}$$

where the radial parameter $\langle r^k e^{-\alpha r}\rangle^{A_1,A_2}$ is the model-independent Barrett moment

$$\begin{aligned}\langle r^k e^{-\alpha r}\rangle^{A_1,A_2}&=(4\pi/Z)\int_0^\infty \rho(r)e^{-\alpha r}r^k r^2 dr\\&=3R_k^{-3}\int_0^{R_k} e^{-\alpha r}r^k r^2 dr\ ,\end{aligned} \tag{12}$$

characterized by the equivalent radius R_k. For the $1s_{1/2}$ muonic state of Yb, $\alpha=0.136$ fm^{-1} and $k=2.340$ [44]. Values of the model-independent parameters $\delta\langle r^k e^{-\alpha r}\rangle^{A_1,A_2}$ and R_k in the case of Yb isotopes have been listed by Clark *et al.* [4] and Engfer *et al.* [48].

The muonic-atom λ^{A_1,A_2} values given in the fourth column of Table VII were deduced from the muonic-atom isotope shifts by Engfer *et al.* and Clark *et al.* assuming a simple (spherically symmetric) Fermi charge distribution of the form [48]

$$\rho(r)=\rho_0\{1+\exp[4\ln3(r-c)/t]\}^{-1}\ , \tag{13}$$

where the change in skin thickness $\delta t^{A_1,A_2}$ was taken to be zero for all isotope pairs. The nuclei of the stable isotopes of Yb have neutron numbers ($N=100$–106) lying approximately midway between the $N=82$ and 126 shell closures, and are known to be strongly deformed, with deformation parameters $\beta\approx0.3$ [44]. Clark *et al.* have shown that the use of a *deformed* Fermi distribution of the form

$$\rho(r,\theta)=\rho_0(1+\exp\{4\ln3[r(1-\beta Y_{20}\cos\theta)-c]\}/t_0)^{-1} \tag{14}$$

yields a spherical average with an "effective skin thickness" given by

$$t_{\rm eff}^2=t_0^2+(4\ln3)^2(3/4\pi^3)c^2\beta^2\ . \tag{15}$$

The relative change in $t_{\rm eff}$ with change in deformation parameter β is then

$$\delta t_{\rm eff}/t_{\rm eff}=\beta\delta\beta/\{\beta^2+[4\pi^3/3(4\ln3)^2](t_0^2/c^2)\}\ . \tag{16}$$

Clark *et al.* have also shown that numerical integration of the Fermi distribution function (13) in the case of Yb with $c=6.37$ fm and $t=2.3$ fm gives

$$\lambda^{A_1,A_2}=45.4\delta c/c+4.95\delta t/t\ . \tag{17}$$

The second term in expression (17), together with $\delta t/t$ from (16), then provides an approximate correction to take account of effects of changes in deformation parameter $\delta\beta$ between pairs of isotopes. From our optical isotope shift results (see Sec. V C below), we find that $\delta\beta$ is negative for all Yb isotope pairs in Table VII, and this reduces the muonic-atom λ^{A_1,A_2} values (column 4) to values (column 5) closer to the optical values. However, λ^{A_1,A_2} is rather sensitive to $\delta\beta$, which introduces large uncertainties in the corrected λ^{A_1,A_2} values.

The electronic x-ray isotope shifts measure essentially the same radial parameter, λ^{A_1,A_2}, as the optical isotope shifts [49]. However, the quoted uncertainties in the x-ray λ^{A_1,A_2} values for Yb are very large (comparable with the differences between the x-ray and optical data) and the quality of the King plot of the electronic x-ray isotope shifts against the optical isotope shifts is very poor (see, e.g., Fig. 4 of Clark *et al.* [4]), indicating that the actual errors in the λ^{A_1,A_2} values are at least as large as the quoted uncertainties. Furthermore, comparison of tabulations of electronic x-ray λ^{A_1,A_2} values [49] and optical isotope shift λ^{A_1,A_2} values [5] suggest that the x-ray results may be much too high for a number of elements.

C. Systematics of Yb nuclei

Figure 4 shows the change in the mean-square radius $\delta\langle r^2\rangle^{152,A_2}$ with increasing neutron number for the chain of 21 ytterbium isotopes listed in Table VI. The increase of $\delta\langle r^2\rangle^{152,A_2}$ with N arises from a combination of a sim-

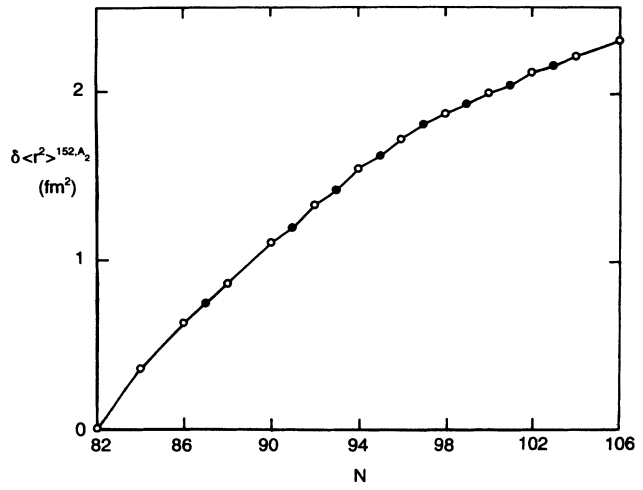

FIG. 4. Change in mean-square nuclear charge radius (relative to ^{152}Yb) vs neutron number for all Yb isotopes for which isotope shift data are available. Open circles refer to even isotopes, and closed circles to odd isotopes. The error bars are smaller than the data points.

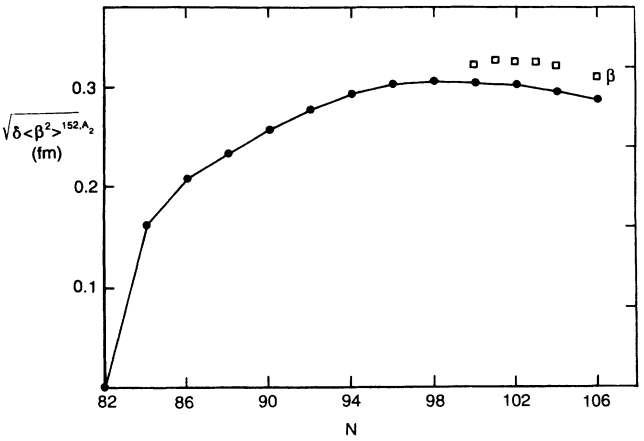

FIG. 5. Square root of the change in mean-square deformation parameter β (relative to ^{152}Yb) vs neutron number for *even* isotopes of Yb. The squares denote absolute values of the charge deformation parameter β deduced from muonic-atom data [44].

ple nuclear volume effect, associated with the increase in total number of neutrons, and a nuclear deformation effect caused by the addition of neutrons to the "spherical" closed-shell nucleus ^{152}Yb ($N=82$).

Following the treatment of Neugart [51], we express $\langle r^2\rangle$ as the sum of a spherical component, $\langle r^2\rangle_0$, and a deformation component characterized by the parameter β:

$$\langle r^2\rangle=\langle r^2\rangle_0+(5/4\pi)\langle r^2\rangle_0\langle\beta^2\rangle \ . \tag{18}$$

Values of the change in the mean-square deformation parameter, $\delta\langle\beta^2\rangle^{152,A_2}$, were then extracted from the $\delta\langle r^2\rangle$ data in Table VI using values for the spherical components, $\delta\langle r^2\rangle_0^{152,A_2}$ and $\langle r^2\rangle_0^{152}=22.1$ fm^2, calculated from the droplet model [52]. Combination of these $\delta\langle\beta^2\rangle^{152,A_2}$ values with absolute β values [44] deduced from muonic atom transition energies (Fig. 5) leads to $(\langle\beta^2\rangle^{152})^{1/2}\approx 0.1$, which seems a reasonable value for the closed-shell nucleus ^{152}Yb. The variation of $(\delta\langle\beta^2\rangle^{152,A_2})^{1/2}$ with neutron number for the *even* Yb isotopes, shown in Fig. 5, reveals an abrupt jump in deformation as the first pair of neutrons is added to the closed-shell nucleus ^{152}Yb ($N=82$). This is then followed by a gradual increase in deformation up to the strongly deformed stable nuclei ^{168,170}Yb (which lie roughly midway between the $N=82$ and 126 shell closures), and then finally a small decrease in deformation from ^{170}Yb ($N=100$) down to ^{176}Yb. The small decrease in deformation between $N=100$ (^{170}Yb) and 106 (^{176}Yb) is responsible for the negative correction term in expression (17), which lowers the muonic-atom λ^{A_1,A_2} values for the stable isotopes of Yb (see Sec. V B).

As pointed out previously [16–18,51,53,54], the behavior of Yb, in which the largest jump in $\delta\langle r^2\rangle^{A_1,A_2}$ occurs immediately after the $N=82$ shell closure, differs markedly from that of the lighter rare earths, $_{68}$Er, $_{66}$Dy, $_{64}$Gd, $_{62}$Sm, $_{60}$Nd, and $_{58}$Ce, all of which exhibit their largest jump between $N=88$ and 90. The sharp jump between $N=88$ and 90 for the lighter rare earths has been interpreted as an effect of the $Z=64$ proton subshell closure, which has a stabilizing influence on the nuclear sphericity for neutron numbers up to 88–90 [18,51,54]. It has been suggested [17,53] that the different behavior in the case of Yb may be associated with the half-filled $h_{11/2}$ proton shell, which seems to respond more easily to the addition of neutrons than the proton configurations of the other rare-earth nuclei.

The variation of $\delta\langle r^2\rangle^{152,A_2}$ with neutron number for Yb (Fig. 4) also exhibits the well-known odd-even staggering effect associated with the neutron pairing energies. The degree of odd-even staggering may be characterized by the parameter [55]

$$\gamma=2\delta\langle r^2\rangle^{A,A+1}/\delta\langle r^2\rangle^{A,A+2} \ , \tag{19}$$

which is unity in the absence of odd-even staggering. Figure 6 shows that γ is close to unity near the $N=82$

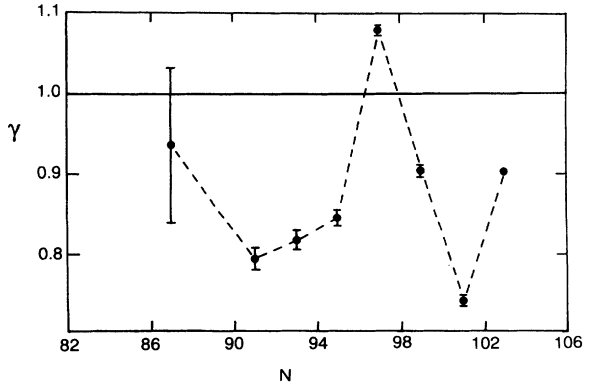

FIG. 6. Odd-even staggering parameter γ vs neutron number for isotopes of Yb.

shell closure, and then decreases to about 0.8 between $N=91$ and 93. At $N=97$, however, γ suddenly jumps to 1.08, which indicates that the centroid of the ^{167}Yb hyperfine components is now actually closer to the heavier even isotope (^{168}Yb) component rather than to the lighter even isotope (^{166}Yb) component. In order to reduce γ to a "normal" value of 0.8, the centroid of the ^{167}Yb components would need to be shifted by about 240 MHz (or 80 times the quoted uncertainty) to the low-frequency side of the reported value [16]. Unfortunately, it is not possible to check the reliability of the isotope shift data using a King plot analysis, since the ^{167}Yb isotope shift has been determined for only one transition (Yb I 555.6 nm), nor is it possible to check the accuracy of the ^{167}Yb magnetic hyperfine structure factor (which might reflect the presence of a large systematic error in the isotope shift) since there does not appear to be any independent measurement of the magnetic moment of ^{167}Yb. However, the 555.6-nm ($6\,^1S_0-6\,^3P_1^o$) transition for ^{167}Yb ($I=\frac{5}{2}$) has only three hyperfine components, and the spectrum was taken from a mass-separated sample [16]; so it is difficult to see how the isotope shift could be in error by as much as 240 MHz. On the other hand, it is also difficult to see why the odd-even staggering should exhibit such a large irregularity in the vicinity of ^{167}Yb ($N=97$), which is far from a shell (or subshell) closure. There is no evidence of a similar effect near $N=97$ in neighboring elements such as $_{66}$Dy [5,51]. The reason for the large irregularity in the odd-even staggering near ^{167}Yb is not clear.

VI. SUMMARY AND CONCLUSIONS

Precision measurements have been made of optical isotope shifts and hyperfine structure in the 369.4-nm $6s$-$6p_{1/2}$ resonance line of the single-valence-electron system Yb^+ using Doppler-free saturated absorption spectroscopy in a sputtered vapor. The isotope shifts have been combined with *ab initio* coupled-cluster calculations of the electronic field shift factor, $F_{6s\text{-}6p_{1/2}}=-14.9(2)$ GHz fm^{-2}, and the specific mass shift factor, $K^{\mathrm{SMS}}_{6s\text{-}6p_{1/2}}=(1\pm1)K^{\mathrm{NMS}}_{6s\text{-}6p_{1/2}}$, to extract values of the nuclear charge distribution parameters, λ^{A_1,A^2} and $\delta\langle r^2\rangle^{A_1,A_2}$, for isotope pairs involving the stable isotopes $^{170\text{-}176}$Yb. The present results have been combined with earlier isotope shift data for the Yb I 555.6-nm line to obtain a set of λ^{A_1,A_2} values involving a chain of 21 nuclei down to the $N=82$ closed-shell nucleus ^{152}Yb. The results indicate that, unlike the other (lighter) rare-earth nuclei, the largest jump in the mean-square charge radius for Yb occurs immediately after the $N=82$ shell closure, and this is followed by a gradual increase in $\delta\langle r^2\rangle^{A_1,A_2}$ up to the (strongly deformed) stable Yb isotopes. A large irregularity is found in the odd-even staggering of $\delta\langle r^2\rangle$ near ^{167}Yb ($N=97$), which is presently not understood.

ACKNOWLEDGMENTS

We wish to thank R. M. Lowe for assistance with the experimental work and B. Klebanowska of the CSIRO Division of Applied Physics for precision measurements of the length of the reference étalon used for the frequency calibration. Funding for the coupled-cluster calculations (A.-M. M.-P.) was provided by the Swedish Natural Science Research Council.

[1] A.-M. Mårtensson-Pendrill, A. Ynnerman, H. Warston, L. Vermeeren, R. E. Silverans, A. Klein, R. Neugart, C. Schulz, P. Lievens, and the ISOLDE Collaboration, Phys. Rev. A **45**, 4675 (1992).

[2] A.-M. Mårtensson-Pendrill and A. Ynnerman, J. Phys. B **25**, L551 (1992).

[3] A. C. Hartley and A.-M. Mårtensson-Pendrill, J. Phys. B **24**, 1193 (1991).

[4] D. L. Clark, M. E. Cage, D. A. Lewis, and G. W. Greenlees, Phys. Rev. A **20**, 239 (1979).

[5] P. Aufmuth, K. Heilig, and A. Steudel, At. Data Nucl. Data Tables **37**, 455 (1987).

[6] R. W. Berends and L. Maleki, J. Opt. Soc. Am. B **9**, 332 (1992).

[7] K. Krebs and H. Nelkowski, Z. Phys. **141**, 254 (1955).

[8] A. F. Golovin and A. R. Striganov, Opt. Spectrosc. **19**, 467 (1965).

[9] Yu Chaiko, Opt. Spectrosc. **20**, 424 (1966).

[10] A. Münch, M. Berkler, Ch. Gerz, D. Wilsdorf, and G. Werth, Phys. Rev. A **35**, 4147 (1987).

[11] R. Casdorff, V. Enders, R. Blatt, W. Neuhauser, and P. E. Toschek, Ann. Phys. (Leipzig) **48**, 41 (1991).

[12] A. Bauch, D. Schnier, and Chr. Tamm (unpublished).

[13] H. Klein, A. S. Bell, G. P. Barwood, and P. Gill, Appl. Phys. B **50**, 13 (1990).

[14] P. T. H. Fisk, M. A. Lawn, and C. Coles, Appl. Phys. B **57**, 287 (1993).

[15] I. Lindgren and J. Morrison, *Atomic Many-Body Theory,* Springer Series in Chemical Physics Vol. 13 (Springer, Berlin, 1982); *ibid.*, 2nd ed., Springer Series on Atoms and Plasmas Vol. 3 (Springer, Berlin, 1986).

[16] F. Buchinger, A. C. Mueller, B. Schinzler, K. Wendt, C. Ekström, W. Klempt, R. Neugart, and the ISOLDE Collaboration, Nucl. Instrum. Methods **202**, 159 (1982).

[17] G. D. Sprouse, J. Das, T. Lauritsen, J. Schecker, A. Berger, J. Billowes, C. H. Holbrow, H.-E. Mahnke, and S. L. Rolston, Phys. Rev. Lett. **63**, 1463 (1989).

[18] J. Billowes, Hyperfine Interact. **59**, 3 (1990).

[19] P. Hannaford, Contemp. Phys. **24**, 251 (1983).

[20] D. S. Gough and P. Hannaford, Opt. Commun. **67**, 209 (1988).

[21] A. P. Willis, D. S. Gough, P. Hannaford, R. M. Lowe, R. J. McLean, and A. Wännström, in *Laser Spectroscopy,* edited by M. Ducloy, E. Giacobino, and G. Camy (World Scientific, Singapore, 1991), pp. 404–405.

[22] J. Migdalek, J. Phys. B **13**, L169 (1980).

[23] R. M. Lowe, P. Hannaford, and A.-M. Mårtensson-Pendrill, Z. Phys. D **28**, 283 (1993).
[24] K. Krebs and H. Nelkowski, Z. Phys. **145**, 543 (1956).
[25] The original values of $\mu_{171}=0.491\,889(8)\mu_N$ and $\mu_{173}=-0.677\,44(3)\mu_N$ reported by Olschewski [26] have since been adjusted to allow for diamagnetic shielding and consistency with the listed standard (^{23}Na) by Lederer and Shirley [27], and the recommended values listed by Lederer and Shirley and also by Raghavan [28] are now $\mu_{171}=0.493\,67(1)\mu_N$ and $\mu_{173}=-0.679\,89(3)\mu_N$. However, the very accurate value for the ratio $\mu_{173}/\mu_{171}=-1.377\,23(7)$ reported by Olschewski [26] should still hold.
[26] L. Olschewski, Z. Phys. **249**, 205 (1972).
[27] C. M. Lederer and V. S. Shirley, *Table of Isotopes,* 7th ed. (Wiley, New York, 1978).
[28] P. Raghavan, At. Data Nucl. Data Tables **42**, 189 (1989).
[29] A. Bohr and V. F. Weisskopf, Phys. Rev. **77**, 94 (1950).
[30] H. H. Stroke, R. J. Blin-Stoyle, and V. Jaccarino, Phys. Rev. **123**, 1326 (1961).
[31] G. Torbohm, B. Fricke, and A. Rosén, Phys. Rev. A **31**, 2038 (1985).
[32] W. H. King, J. Opt. Soc. Am. **53**, 638 (1963).
[33] H. Kopfermann, *Nuclear Moments* (Academic, New York, 1958).
[34] J. Bauche, Comments At. Mol. Phys. **10**, 57 (1981).
[35] S. Salomonson and P. Öster, Phys. Rev. A **40**, 5548 (1989).
[36] V. Kaufmann and J. Sugar, J. Opt. Soc. Am. **63**, 1168 (1973).
[37] K. Koc and J. Migdalek, J. Phys. B **25**, 907 (1992).
[38] B. C. Fawcett and M. Wilson, At. Data Nucl. Data Tables **47**, 241 (1991).
[39] T. H. Schucan and H. A. Weidenmüller, Ann. Phys. (N.Y.) **73**, 108 (1972); **76**, 483 (1973).
[40] I. Lindgren, Nucl. Instrum. Methods B **31**, 102 (1988).
[41] I. Lindgren, J. Phys. B **7**, 2441 (1974).
[42] In earlier work [2,3], the results were quoted as $F(1-\kappa)$, whereas the numbers in Table IV are actual F values.
[43] A detailed presentation is found in L. Armstrong, Jr., *Theory of the Hyperfine Structure of Free Atoms* (Wiley-Interscience, New York, 1971).
[44] We note that the numbers given for $F_{p_{3/2}}$ by Mårtensson-Pendrill and Ynnerman [2] are too large by a factor of $\sqrt{2}$.
[45] A. Zehnder, F. Boehm, W. Dey, R. Engfer, H. K. Walter, and J. L. Vuilleumier, Nucl. Phys. A **254**, 315 (1975).
[46] R. W. Berends, E. H. Pinnington, B. Guo, and Q. Ji, J. Phys. B **26**, L701 (1993).
[47] J. Bauche, Ph.D. thesis, Université de Paris, 1969; J. Phys. (Paris) **35**, 19 (1974).
[48] R. Engfer, H. Schneuwly, J. L. Vuilleumier, H. K. Walter, and A. Zehnder, At. Data Nucl. Data Tables **14**, 509 (1974).
[49] F. Boehm and P. L. Lee, At. Data Nucl. Data Tables **14**, 605 (1974).
[50] P. L. Lee and F. Boehm, Phys. Rev. C **8**, 819 (1973).
[51] R. Neugert, in *Lasers in Nuclear Physics,* edited by C. E. Bemis and H. J. Carter (Harwood Academic, New York, 1982), p. 231.
[52] W. D. Myers, Phys. Lett. **30B**, 451 (1969).
[53] C. H. Holbrow, G. D. Sprouse, J. Das, J. Schecker, T. Lauritsen, J. Billowes, A. Berger, F. Xu, and W. Kim, Nucl. Instrum. Methods Phys. Res. B **56/57**, 528 (1991).
[54] R. Neugart, K. Wendt, S. A. Ahmad, W. Klempt, C. Ekström, and the ISOLDE Collaboration; Hyperfine Interact. **15/16**, 181 (1983).
[55] P. Aufmuth and M. Haunert, Physica **123C**, 109 (1983).
[56] R. Blatt, H. Schnatz, and G. Werth, Z. Phys. A **312**, 143 (1983).
[57] A.-M. Mårtensson-Pendrill and A. Ynnerman, Phys. Scr. **41**, 329 (1990).